International Journal of Mechanical Sciences 89 (2014) 194–206

Contents lists available at ScienceDirect

International Journal of Mechanical Sciences

journal homepage: www.elsevier.com/locate/ijmecsci

Lyapunov exponents of impact oscillators with Hertz's and Newton's contact models

Wioleta Serweta [a], Andrzej Okolewski [b], Barbara Blazejczyk-Okolewska [a,*], Krzysztof Czolczynski [a], Tomasz Kapitaniak [a]

[a] Division of Dynamics, Lodz University of Technology, Stefanowskiego 1/15, 90-924 Lodz, Poland
[b] Institute of Mathematics, Lodz University of Technology, Wolczanska 215, 90-924 Lodz, Poland

ARTICLE INFO

Article history:
Received 24 March 2014
Received in revised form
28 August 2014
Accepted 12 September 2014
Available online 20 September 2014

Keywords:
Impact oscillator
Cantilever beam system
Hertz contact models
Newton contact model
Lyapunov exponents

ABSTRACT

In this paper, investigations of a harmonically excited one-degree-of-freedom mechanical system having an amplitude constraint are presented. The contact between the oscillated mass and the barrier is modeled by Hertz's law with a non-linear damping as well as by Newton's law. The influence of the frequency of excitation force on the system's behavior is studied in a wide range of the control parameter by determining and analyzing the corresponding spectra of Lyapunov exponents. The dynamical behaviors of two systems with impacts: a system with Hertz's undamped impacts and a system with perfectly elastic hard impacts, which are equivalent in the sense of the same rate of impact energy dissipation, are compared and strong qualitative and quantitative similarities are observed. As an application example, a simple cantilever beam system with impacts is considered and the combined effects of the nonlinearities due to beam deflection and impacts of Hertz's as well as Newton's types are investigated.

1. Introduction

The calculation of Lyapunov exponents is one of fundamental elements in analysis of nonlinear dissipative systems with a finite number of degrees of freedom. They are numerical characteristics that allow for qualitative and quantitative evaluation of the system dynamics. These quantities are strictly connected to such measures of chaos as the Kolmogorov entropy and dimension of the dynamical system. The theoretical foundations for existence and uniqueness of Lyapunov exponents have been presented by Oseledec [1]. A spectrum of Lyapunov exponents characterizes the medium expansion of a small subset in the phase space along the trajectory. To identify the character of the system dynamics, it is usually enough to know the sign of the largest Lyapunov exponent—its non-positiveness renders the regularity of the system motion, whereas its positiveness—proves the chaotic character of the solution. The value of the largest Lyapunov exponent describes the rate of the mean exponential convergence or divergence of adjacent trajectories on the attractor.

The first method to calculate the whole spectrum of Lyapunov exponents was presented independently by Benettin et al. [2] and Shimada and Nagashima [3]. In the literature, there are two classical approaches towards determination of Lyapunov exponents for smooth systems with known equations of motion. In the first one, (see, for instance, [4]), an evolution of infinitesimal vectors of distortions in the trajectory under consideration is described by means of linearization of the vector field. The second approach (see, for example, [5]) consists in a substitution of the continuous system by its discrete counterpart, for instance, by applying Poincare maps, and a consideration of the linearization of the discrete map. Some alternative methods proposed by Stefanski (see, for instance, [6]) and Dabrowski (see, [7]) allow for determination of the largest Lyapunov exponent on the basis of the synchronization phenomenon of pairs of identical systems and the derivative dot product of perturbation vector, respectively.

Methods that enable estimation of Lyapunov exponents from experimental time series, that is to say, in the case when the system of differential equations describing the behavior of the system is not available, are known as well. Their basis usually lies in a reconstruction of the state space with the delay method, introduced by Takens [8]. The first procedure of this kind for calculation of the largest Lyapunov exponent was given by Wolf et al. [9], whereas analogous algorithms for determination of the whole spectrum of Lyapunov exponents can be found in Parlitz [10], Sano and Sawada [11], and Yang and Wu [12].

In the literature, a few adaptations of classical methods for determination of Lyapunov exponents to the case of piecewise smooth systems can be found. Müller [13] (cf [14]) has shown that

* Corresponding author. Tel.: +48 426312233; fax: +48 426365646.
E-mail address: okolbar@p.lodz.pl (B. Blazejczyk-Okolewska).

http://dx.doi.org/10.1016/j.ijmecsci.2014.09.007
0020-7403/

the conditions for transition of the system through the non-smoothness have their counterparts for the linearized system, due to which it is possible to determine Lyapunov exponents with a classical method of the Benettin et al. type [2]. A similar modification of the discrete method, based on the notion of local Nordmark maps [15], has been presented by Jin et al. [16]. A different approach with a smaller range of applications limited to piecewise linear systems, consists in an application of discontinuity maps ([17,18]) instead of Poincare maps.

An important part of the dynamical systems is represented by those systems whose motions take place in the presence of impacting interactions between the masses of the system (see [19,20]). The classic approach to study the collision process, called stereomechanical model of a collision [21] or hard collision model [22], uses the coefficient of restitution and the principle of conservation of momentum, and allows to determine the velocity of the bodies after the collision on the basis of knowledge of the velocity of the bodies before the collision. Taking into account the duration of the impact and the coefficient of restitution depending on the velocity, leads to models which more accurately describe the process of collision (see e.g. [23,24]). Such a process is similar to the collision with the stop with a certain vulnerability, and is called a soft collision model [22]. In this case, there is a choice of stops modeling. They can be linear (e.g., models of vibroimpact systems with clearance [25–28]) or nonlinear (e.g., Hertz's models [21,29,30]), elastic or elastic-damping constructions. A comprehensive survey of the current knowledge about systems with impacts has been made by Ibrahim [31].

The above-described methods of deriving Lyapunov exponents have been applied to impact systems with rigid stops ([32–36]), except for [37], in which Lyapunov exponents have been calculated with the method of impact maps for piecewise linear one-degree-of-freedom systems with one-sided impacts.

In this paper, we deal with a one-degree-of-freedom linear oscillator with impacts modeled with soft nonlinear elastic structures (Hertz's contact model [21]), soft nonlinear elastic-damping structures (Hertz's damp contact model [30]) as well as Newton's law of contact, which besides its own interest, aims at representing an impacting cantilever beam system. The main objective is to analyze qualitatively and quantitatively the influence of the frequency of excitation force on the system's behavior in the case of these three contacts models as well as to compare the resulting responses. To this aim, we adapt the Müller's approach and determine numerically the spectra of Lyapunov exponents. The results obtained are consistent with the corresponding bifurcation diagrams.

The presented study shows that the knowledge of Lyapunov exponents enables more detailed analysis of the system's behavior in comparison to other tools, e.g., Poincare maps or bifurcation diagrams. In particular, it allows to identify some phenomena which have not been reported on the basis of bifurcation diagrams, like some periodic orbits not identified in the study by Pust and Peterka [30]. Furthermore, we show that Lyapunov exponents can provide a tool for not only qualitative (cf. [29]) but also quantitative comparison of different systems with impacts. The presented comparison of dynamical behaviors of a system with Hertz type undamped collisions of relatively small values of stiffness and a system with perfectly elastic hard collisions revealed their good qualitative and quantitative agreement. This agreement manifests itself in the appearance, for almost the same values of the excitation force, of the chaotic motions with almost identical values of the Lyapunov exponents corresponding to both the collisions models, as well as in the existence, in a wide range of the excitation force, of periodic motions with impacts, for which the corresponding Lyapunov exponents are very close to each other. In particular, this is the case when the two systems begin to come into collisions with low velocity impacts, causing instabilities of grazing-type.

From the mechanical engineering point of view, our results apply to a simple cantilever beam system with impacts, which is commonly used as an element of engineering design. However, if the beams are parts of a larger system, significant errors in the dynamical responses can result from neglecting even small nonlinearities. The cumulative effect of the nonlinearity associated with the beam deflection and the nonlinearity due to impact model with clearance and linear spring was examined by Emans et al. [38] and Lin et al. [39]. We extend these studies to two other impact models. A comparison of dynamic responses of simple linear and nonlinear beam systems with impacts of Hertz's and Newton's type revealed their qualitative differences for physically realistic parameters.

This paper is organized as follows. Mathematical models of the considered system are introduced in Section 2. In Sections 3 and 4, the classical method for Lyapunov's exponents determination as well as its modification for systems with singularities are briefly described. Analysis of a harmonically excited one-degree-of-freedom impact oscillator with two Hertz's models of contact carried out with the help of the corresponding spectra of Lyapunov's exponents as well as a comparison of dynamics of a system with perfectly elastic hard impacts and an equivalent, in the sense of the same rate of impact energy dissipation, system with Hertz's impacts, are presented in Section 5. In Section 6, the cumulative effect of different type nonlinearities on cantilever beam responses is investigated. The conclusions are formulated in Section 7.

2. Mathematical model of the system

The system under consideration consists of a linear oscillator with mass m, coefficient of viscous damping c and spring stiffness coefficients k and k_e, presented in Fig. 1. The oscillator can be under either external kinematic excitation (Fig. 1a) or external forcing (Fig. 1b). In the first case the upper end of the spring k_e moves harmonically with the assigned amplitude a and frequency ω. In the second case, the harmonic force of the assigned amplitude F and frequency ω acts on the oscillator. When the oscillators are in their static equilibrium positions, the distance between their impacting surfaces and the unmovable fender is ρ. The motion of the oscillators around their static equilibrium positions is described by coordinate x.

The equations of impactless motion of the above-described systems are as follows:

– for the oscillator shown in Fig. 1a

$$m\frac{d^2x}{dt^2}+c\frac{dx}{dt}+(k+k_e)x=k_e a\cos\omega t, \quad (1a)$$

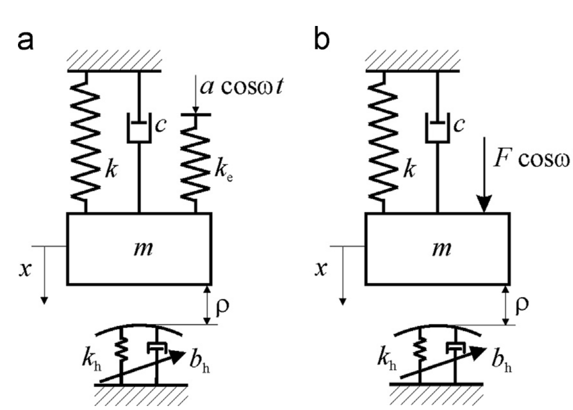

Fig. 1. Impacting oscillators with two types of external excitation.

– for the oscillator shown in Fig. 1b

$$m\frac{d^2x}{dt^2}+c\frac{dx}{dt}+kx=F\cos\omega t. \tag{1b}$$

Dividing both sides of Eq. (1a) by $(k+k_e)a$ and introducing dimensionless time $\tau=\alpha t$, one obtains this equation in the dimensionless form:

$$X''+2bX'+X=\xi\cos\eta\tau, \tag{2a}$$

where $\alpha=\sqrt{(k+k_e)/m}$ is the frequency of free vibrations of the undamped system, $b=c/(2\sqrt{(k+k_e)m})$—dimensionless damping, related to the critical one, $\xi=k_e/(k+k_e)$—relation between the stiffness coefficients, $\eta=\omega/\alpha$—dimensionless frequency of forcing, $X=x/a$—dimensionless displacement related to the amplitude of kinematic forcing and X' denotes the derivative $dX/d\tau$. The dimensionless distance between the oscillator and the fenders $r=\rho/a$.

Dividing both sides of Eq. (1b) by F and introducing dimensionless time $\tau=\alpha t$, yields this equation in the dimensionless form:

$$X''+2bX'+X=\cos\eta\tau, \tag{2b}$$

where $\alpha=\sqrt{k/m}$, $b=c/(2\sqrt{km})$, $\eta=\omega/\alpha$, $X=x/x_{st}$—dimensionless displacement related to the static displacement $x_{st}=F/k$. The dimensionless distance $r=\rho/x_{st}$. After these transformations, both the considered systems can be shown in dimensionless form presented in Fig. 2.

For appropriately selected parameters of the system, there is a possibility of contact of the mass with the stop, i.e. deflection of the mass of ρ (Fig. 1) or r (Fig. 2). In this paper, a continuation of the research on the dynamic of the systems with soft stops with nonlinear characteristics (see [29,30]) is conducted in the case of two special nonlinear contact models. The equations describing the motion of the system are then supplemented with the appropriate collision force.

2.1. Hertz's contact model

The most popular Hertz's model of contact is the non-linear elastic model in which the collision force F_ρ is of the form:

$$\begin{aligned} &F_\rho=0 && x<\rho,\\ &F_\rho=k_h(x-\rho)^{3/2} && x\geq\rho, \end{aligned} \tag{3a}$$

where k_h is the ratio of the stiffness of the surface, dependent on the elastic properties and geometry of the colliding bodies. A rich source of information on the stiffness coefficient k_h is, for example, the monograph by Goldsmith [21].

Let us introduce the dimensionless variables: $k_H=(k_h\sqrt{a})/(k+k_e)$ for the system (1a), and $k_H=(k_h\sqrt{x_{st}})/k$ for the system (1b). Then (3a) takes the following dimensionless form:

$$\begin{aligned} &F_r=0, && X<r,\\ &F_r=k_H(X-r)^{3/2} && X\geq r. \end{aligned} \tag{3b}$$

2.2. Hertz's damp contact model

As impacts in real systems are always accompanied with loss of energy, the damping b_h has to be included in corresponding mathematical models. There are various Hertz-type laws with nonlinear damping which have been studied in the literature (see, e.g., [30,31,40,41]). In the sequel, we will consider the following model:

$$\begin{aligned} &F_\rho=0 && x<\rho,\\ &F_\rho=k_h(x-\rho)^{3/2}(1+b_h\dot{x}) && x\geq\rho, \end{aligned} \tag{4a}$$

which has been discussed by Pust and Peterka [30].

Introducing dimensionless variables: $k_H=(k_h\sqrt{a})/(k+k_e)$, $b_H=b_h a\alpha$ for the system (1a), and $k_H=(k_h\sqrt{x_{st}})/k$, $b_H=b_h x_{st}\alpha$ for the system (1b) we obtain the following dimensionless counterparts of (4a):

$$\begin{aligned} &F_r=0 && X<r,\\ &F_r=k_H(X-r)^{3/2}(1+b_H X') && X\geq r, \end{aligned} \tag{4b}$$

2.3. Dimensionless systems of equations of the first order

The dynamics of systems described by the second order differential equations can be reduced to the analysis of the systems of the first order differential equations:

$$\frac{dx_i}{dt}=f_i(t,x_1,\ldots,x_n), \quad i=1,\ldots,n. \tag{5}$$

The systems of differential equations corresponding to the Eqs. (2a) and (2b), respectively, have the following forms:

$$\begin{aligned} &\dot{x}_1=x_2\\ &\dot{x}_2=\xi\cos\eta\tau-2bx_2-x_1-F_r, \end{aligned} \tag{6a}$$

and

$$\begin{aligned} &\dot{x}_1=x_2\\ &\dot{x}_2=\cos\eta\tau-2bx_2-x_1-F_r, \end{aligned} \tag{6b}$$

where F_r denotes the collision force. In the case of Hertz's model of contact the collision force is given as follows:

$$\begin{aligned} &F_r=0 && x_1<r\\ &F_r=k_H(x_1-r)^{3/2} && x_1\geq r, \end{aligned} \tag{7a}$$

while in the case of Hertz's damp model of contact the force has the form:

$$\begin{aligned} &F_r=0 && x_1<r\\ &F_r=k_H(x_1-r)^{3/2}(1+b_H x_2) && x_1\geq r. \end{aligned} \tag{7b}$$

3. The definition of Lyapunov exponents and a method of their determination

Consider a dynamical system which evolves according to the following equation:

$$\dot{\mathbf{x}}=\mathbf{f}(\mathbf{x}), \quad \mathbf{x}(t_0)=\mathbf{x}_0, \tag{8}$$

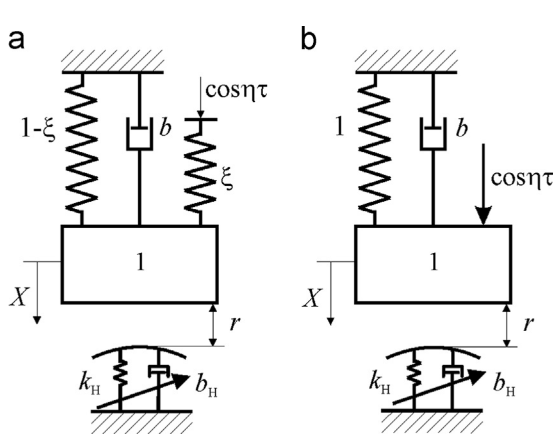

Fig. 2. Impacting oscillators—dimensionless form.

where $\mathbf{x} = [x_1, \dots, x_n]^T \in D \subset R^n$ is the state vector, $\mathbf{f} = [f_1, \dots, f_n]^T$ is the continuously differentiable vector field and t_0 is the initial time. Let $y(t)$ be a particular solution of the system (8) and $\overline{y}(t)$ be a perturbed solution. Define the difference between the perturbed solution and the particular solution as $\delta y(t) = \overline{y}(t) - y(t)$. The time evolution of $\delta y(t)$ is governed by the linearized equation:

$$\delta \dot{y}(t) = D\mathbf{f}(y(t))\delta y \,, \tag{9}$$

where

$$D\mathbf{f}(y(t)) = \left.\frac{\partial \mathbf{f}(\mathbf{x})}{\partial \mathbf{x}}\right|_{\mathbf{x} = y(t)}$$

is the Jacobi matrix of $\mathbf{f}$ at point $\mathbf{x} = y(t)$.

The solution of (9) can be expressed as follows:

$$\delta y(t) = \mathbf{\Phi}_t(\mathbf{x}_0)\delta y(t_0), \tag{10}$$

where $\mathbf{\Phi}_t(\mathbf{x}_0)$ stands for the solution of the variational equation:

$$\dot{\mathbf{\Phi}}_t(\mathbf{x}_0) = D\mathbf{f}(y(t))\mathbf{\Phi}_t(\mathbf{x}_0), \quad \mathbf{\Phi}_{t_0}(\mathbf{x}_0) = \mathbf{I}, \tag{11}$$

where $\boldsymbol{I}$ denotes the identity matrix of the dimension $n \times n$.

The Eq. (11) is a matrix-valued time-varying linear differential equation. It is the linearization of the vector field along the trajectory $y(t)$. The Lyapunov exponents can be defined as the following limits:

$$\lambda_i = \lim_{t \to \infty} \frac{1}{t} \ln |m_i(t)|, \tag{12}$$

whenever the limits exist, where $m_i(t)$ are the eigenvalues of $\mathbf{\Phi}_t(\mathbf{x}_0)$.

The definition (12) cannot be directly used in the numerical calculations because for large t's the matrix $\mathbf{\Phi}_t(\mathbf{x})$ tends to be ill-conditioned and in consequence the $m_i(t)$ cannot be determined reliably. In addition, for a chaotic system at least one Lyapunov exponent is positive which implies that $\mathbf{\Phi}_t(\mathbf{x})$is unbounded as $t \to \infty$. In order to omit such problems, one can apply the iterative approach proposed by Benettin et al. [2] (see, e. g., the monograph Parker and Chua [4] for the corresponding algorithm), which is based on the Gram–Schmidt orthonormalization procedure. This method can be successfully used to calculate the Lyapunov exponents of autonomous as well as non-autonomous systems. However, its applicability is limited by the requirement of smoothness of the system (8) throughout the considered time period ($\mathbf{f}$ has to be continuously differentiable). Non-smoothness and in particular discontinuity in the equations of motion make the linearization of the system according to Eqs. (9)–(11) impossible.

Among mechanical systems there exists the important class of systems which cannot be described by equations with a single continuously differentiable function $\mathbf{f}$. A good example would be the systems with friction or the systems with impacts. In the case of such systems, the linearization of the equations of motion has to be accompanied by certain conditions for passing through a singularity. They will be briefly described in the following section.

4. Müller's procedure and its adaptation to the systems under consideration

Consider a dynamical system with singularities whose behavior in intervals between instances of singularities $t_0 < t_1 < t_2 < \dots$ (by convention, we treat the initial time t_0 as a singularity instant) and at the ends of these intervals describe the following equations (cf. [13]):

$$t_{i-1} < t < t_i: \quad \dot{\mathbf{x}} = \mathbf{f}_i(\mathbf{x}), \quad \mathbf{x}(t_{i-1}) = \mathbf{x}^{(i-1)+}, \tag{13}$$

$$t = t_i: \quad 0 = \mathbf{h}(\mathbf{x}^{i-}), \tag{14}$$

$$\mathbf{x}^{i+} = \mathbf{g}(\mathbf{x}^{i-}), \tag{15}$$

$$t_i < t < t_{i+1}: \quad \dot{\mathbf{x}} = \mathbf{f}_{i+1}(\mathbf{x}), \quad \mathbf{x}(t_i) = \mathbf{x}^{i+}, \tag{16}$$

where $\mathbf{x}^{0+} = \mathbf{x}_0$, $i = 1, 2, \dots$, $\mathbf{f}_i$, $\mathbf{g}$ and $\mathbf{h}$ are continuously differentiable vector functions, while $\mathbf{x}^{i-} = \lim_{t \uparrow t_i} \mathbf{x}(t)$ and $\mathbf{x}^{i+} = \lim_{t \downarrow t_i} \mathbf{x}(t)$, respectively, are the state vector at the time immediately before the ith point of singularity and the state vector immediately after the ith point of singularity. In each interval (t_{i-1}, t_i) the system behaves smoothly and its motion is described by Eq. (13). The singularity instants $t_1, t_2, \dots$ are determined by zeros of the smooth function $\mathbf{h}(\mathbf{x})$, i.e. by Eq. (14); the function $\mathbf{h}(\mathbf{x})$ can be scalar or vector. At each time $t = t_i$, the state of the system changes according to rules (15) defined by the smooth function $\mathbf{g}(\mathbf{x})$ as well as the vector field changes from $\mathbf{f}_i$ to $\mathbf{f}_{i+1}$ (provided that $\mathbf{f}_i \neq \mathbf{f}_{i+1}$). In consequence, for $t \in (t_i, t_{i+1})$ the system is governed by Eq. (16). The perturbed trajectory $\overline{\mathbf{x}}(t) = \mathbf{x}(t) + \delta\mathbf{x}(t)$, which is close to the unperturbed trajectory $\mathbf{x}(t)$, reaches the corresponding singularity at the instant $\overline{t}_i$ other than t_i, i.e.

$$\overline{t}_i = t_i + \delta t_i \tag{17}$$

and the following equations are satisfied as follows:

$$\overline{t}_{i-1} < t < \overline{t}_i: \quad \dot{\overline{\mathbf{x}}} = \mathbf{f}_i(\overline{\mathbf{x}}), \quad \overline{\mathbf{x}}(\overline{t}_{i-1}) = \overline{\mathbf{x}}^{(i-1)+}, \tag{18}$$

$$t = \overline{t}_i: \quad 0 = \mathbf{h}(\overline{\mathbf{x}}^{i-}), \tag{19}$$

$$\overline{\mathbf{x}}^{i+} = \mathbf{g}(\overline{\mathbf{x}}^{i-}), \tag{20}$$

$$\overline{t}_i < t < \overline{t}_{i+1}: \quad \dot{\overline{\mathbf{x}}} = \mathbf{f}_{i+1}(\overline{\mathbf{x}}), \quad \overline{\mathbf{x}}(\overline{t}_i) = \overline{\mathbf{x}}^{i+}, \tag{21}$$

where $\overline{\mathbf{x}}^{i-} = \lim_{t \uparrow \overline{t}_i} \overline{\mathbf{x}}(t)$ and $\overline{\mathbf{x}}^{i+} = \lim_{t \downarrow \overline{t}_i} \overline{\mathbf{x}}(t)$.

If the indicator function defining the singularity instants is a scalar function, then

$$\delta t_i = -\frac{D\mathbf{h}(\mathbf{x}^{i-})\delta\mathbf{x}^{i-}}{D\mathbf{h}(\mathbf{x}^{i-})\mathbf{f}_i(\mathbf{x}^{i-})}, \tag{22}$$

in which

$$D\mathbf{h}\left(\mathbf{x}^{i-}\right) = \left.\frac{\partial \mathbf{h}(\mathbf{x})}{\partial \mathbf{x}}\right|_{\mathbf{x} = \mathbf{x}^{i-}}$$

is the Jacobi matrix of $\mathbf{h}$ at point $\mathbf{x}^{i-}$. The value of the perturbation immediately after the instant of singularity

$$\delta\mathbf{x}^{i+} = D\mathbf{g}\left(\mathbf{x}^{i-}\right)\delta\mathbf{x}^{i-} + \left(D\mathbf{g}\left(\mathbf{x}^{i-}\right)\mathbf{f}_i\left(\mathbf{x}^{i-}\right) - \mathbf{f}_{i+1}\left(\mathbf{x}^{i+}\right)\right)\delta t_i \,, \tag{23}$$

where δt_i is given by the Eq. (22), $\delta\mathbf{x}^{i-}$ denotes the value of the perturbation immediately before the instant of singularity and $D\mathbf{g}(\mathbf{x}^{i-})$ stands for the Jacobi matrix of the function $\mathbf{g}$ at point $\mathbf{x}^{i-}$ ([33]). Note that the perturbation may experience abrupt changes even when the considered trajectory is continuous, but it is nonsmooth.

Knowing the initial condition $\delta\mathbf{x}(t_{i-1}) = \delta\mathbf{x}^{(i-1)+}$, we can integrate the Eq. (9) with $\mathbf{f}_i$ inserted instead of $\mathbf{f}$ over the interval (t_{i-1}, t_i), and then, based on the knowledge of the vector $\delta\mathbf{x}^{i-} = \lim_{t \uparrow t_i} \delta\mathbf{x}(t)$, that is, the value of perturbation at the end of the interval, we can determine the value of the perturbation $\delta\mathbf{x}^{i+}$, which enables the continuation of calculations, i.e. integration of (9) over the interval (t_i, t_{i+1}) with $\mathbf{f}_{i+1}$ written in place of $\mathbf{f}$ and with the initial condition $\delta\mathbf{x}(t_i) = \delta\mathbf{x}^{i+}$.

The classical algorithm for calculating Lyapunov's exponents of smooth equations of motion by Benettin et al. [2] along with the modifications taking into account abrupt changes of the vector field and perturbation vector at points of singularities has been tested numerically and used to analyze the Eqs. (2a) and (2b) with Hertz's model of contact (4), Hertz's damp contact model (6) and Newton's impact model. For the first two contact models, $\mathbf{f}_{2i-1}$

and $\mathbf{f}_{2i}$ corresponds to $\mathbf{f}$ given by (6a) and (6b) with zero and nonzero F_r, respectively, and the Jacobi matrices of the corresponding functions $\mathbf{h}(\mathbf{x}) = x_1 - r$ and $\mathbf{g}(\mathbf{x}) = [x_1, x_2]$ at the instants immediately after the singularity are of the

$$D\mathbf{h}\left(\mathbf{x}^{i+}\right) = [1, 0] \tag{24}$$

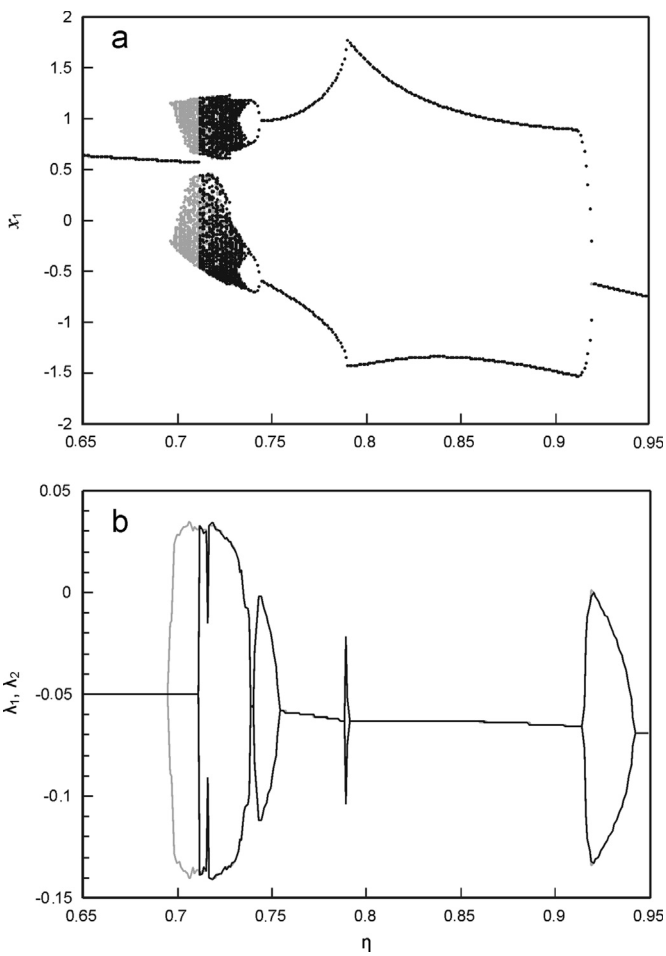

Fig. 3. Bifurcation diagrams of displacements x_1 (a) and corresponding spectra of Lyapunov exponents λ_1, λ_2 (b) for Hert'z damp impact model with: $b=0.05$, $\rho=2$, $k_H=100$, $b_H=0.1$ and $\xi=1$; $\Delta\eta=0.001$.

and

$$D\mathbf{g}\left(\mathbf{x}^{i+}\right) = \begin{bmatrix} \frac{\partial g_1}{\partial x_1} & \frac{\partial g_1}{\partial x_2} \\ \frac{\partial g_2}{\partial x_1} & \frac{\partial g_2}{\partial x_2} \end{bmatrix} = \begin{bmatrix} 1 & 0 \\ 0 & 1 \end{bmatrix}. \tag{25}$$

The Jacobi matrix (25) is the unit diagonal matrix. This reflects the fact that in the case of impact oscillator with Hertz's model of contact, the structure of vector field changes, but the velocity and the displacement remain unchanged at the instant of collision. It is in contrast to the hard impacts modeled by the coefficient of restitution k_r, where the vector field does not changes, but the velocity changes at the moment of collision. In the latter case, there is the following relation between the velocity of the mass before the collision x_2^- and its velocity after collision x_2^+:

$$x_2^+ = -k_r x_2^-, \tag{26}$$

which is known as Newton's law of impacts. Then the functions $\mathbf{f}_i$ are equal to each other for all i, the function $\mathbf{h}$ is the same as for Hertz's contact model, while $\mathbf{g}(\mathbf{x}) = [x_1, -k_r x_2]$, which implies that

$$D\mathbf{g}\left(\mathbf{x}^{i+}\right) = \begin{bmatrix} 1 & 0 \\ 0 & -k_r \end{bmatrix}.$$

Within the framework of Hertz's law of impact, the ratio x_2^+/x_2^- is called the equivalent coefficient of restitution. Since the value of this ratio depends on x_2^-, a system with hard impacts and a system with Hertz's impacts can be equivalent in the sense of the same rate of impact energy dissipation only when the ratio is equal to 1, i.e. when there is no damping caused by impacts in these two systems (cf. Pust and Peterka [30]).

5. Lyapunov exponents and dynamics of linear oscillator with Hertz's and Newton's impacts

The investigations were carried out by means of numerical simulation of the system mathematical model. The ordinary differential equations were solved using a modified Runge–Kutta method, commonly known as the Runge–Kutta–Gill (RKG) method. This method was employed to integrate the equations of motion with the constant time-step between impacts. In the vicinity of impact, special algorithms were used that change the computational step of RKG so that the instant of appearance of impact was determined very precisely. In order to find precisely the instant of impact, the Newton iterative method was applied.

The upper part of Fig. 3a presents the bifurcation diagram of system (6a) and (6b) for typical system parameters $b=0.05$, $\rho=2$,

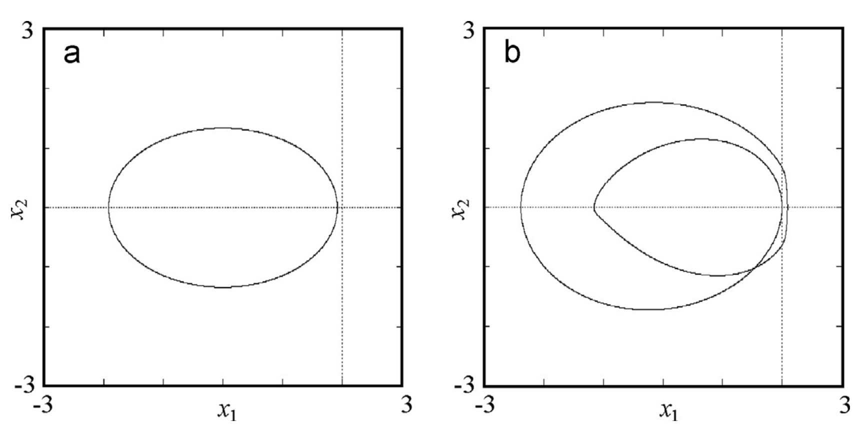

Fig. 4. Phase trajectories of coexisting attractors for $\eta=0.696$, $b=0.05$, $\rho=2$, $k_H=100$, $b_H=0.1$ and $\xi=1$: (a) impactless motion for the initial conditions $x_1=0.591$, $x_2=-1.273$ ($\lambda_1=-0.050$, $\lambda_2=-0.050$); (b) period-2 motion ($z=1/2$) for $x_1=1.153$, $x_2=-1.332$ ($\lambda_1=-0.015$, $\lambda_2=-0.089$).

$k_H=100$, $b_H=0.1$ and $\xi=1$. The frequency η of the excitation force is presented on the horizontal axis, whereas the vertical axis shows the displacement of the system x_1. The results were simulated numerically at the increasing and decreasing frequency in small step $\Delta\eta=0.001$. After each step, the last solution was used as a new initial value. Thus, we can observe the attractor (after the transitional time $T_\eta=5000\cdot T;\quad T=2\pi/\eta$) on the diagram during the complete time of its existence (we say that we move along the attractor), and coexisting attractors can be identified due to the hysteresis region that appears. Fig. 3a is supplemented (see its lower part—Fig. 3b) by spectra of Lyapunov's exponents characteristics $(\lambda_1, \lambda_2)(\eta)$. They were determined according to the procedure described in Sections 3 and 4 with the ortonormalization time $T_o=15\cdot T$ and absolute convergence precision $\varepsilon=0.000001$ (cf. [4]). The basic criterion of distinguishing between the various kinds of motion was the quantity $z=p/n$, where p is the number of impacts in the motion period and n is the number of excitation force periods T in the motion period.

For the same set of parameters, the system (6a) was analyzed in terms of amplitude by Pust and Peterka [30]. In this paper we first show that the spectrum of Lyapunov exponents is a tool that allows for more precise analysis of the dynamics of systems with impacts as the knowledge of these quantities allows to identify the attractors which have not been detected by other methods in [30].

Analyzing the dynamics of the system we can see that for a wide range of the control parameter η, the system exhibits identical behavior with the increase as well as the decrease of the parameter. Such a behavior is obviously recorded for $\eta\in$

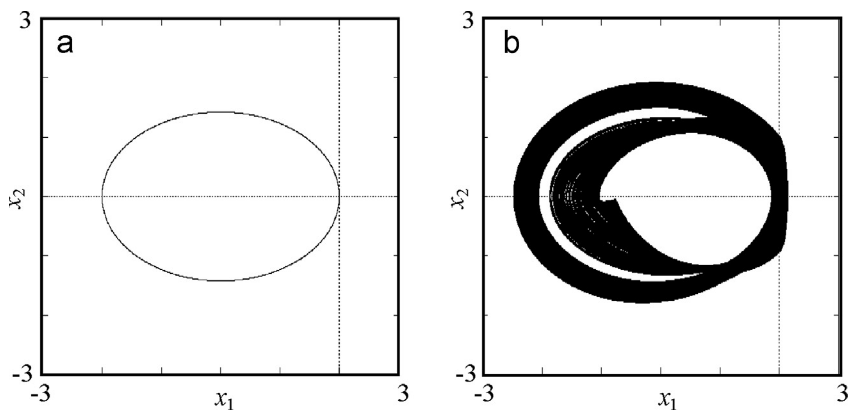

Fig. 5. Phase trajectories of coexisting attractors for $\eta=0.711$, $b=0.05$, $\rho=2$, $k_H=100$, $b_H=0.1$ and $\xi=1$: (a) impactless motion for the initial conditions $x_1=0.575$, $x_2=-1.363$ ($\lambda_1=-0.050$, $\lambda_2=-0.050$); (b) chaotic motion for the initial conditions $x_1=-0.379$, $x_2=-0.717$ ($\lambda_1=0.031$, $\lambda_2=-0.136$).

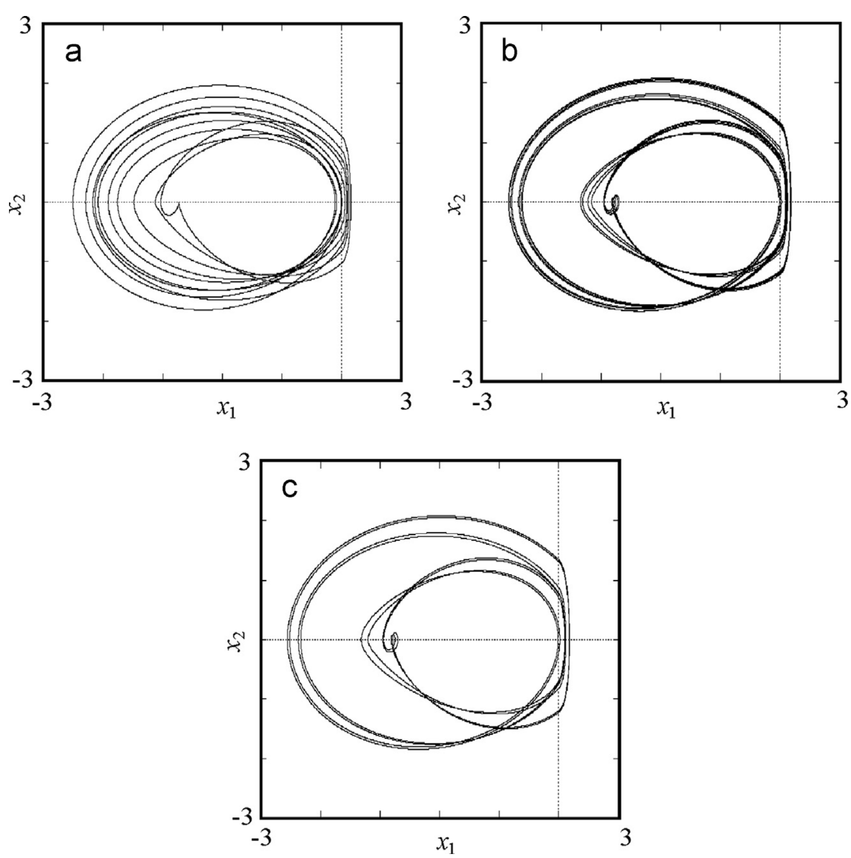

Fig. 6. Phase trajectories of periodic solutions for $b=0.05$, $\rho=2$, $k_H=100$, $b_H=0.1$ and $\xi=1$: (a) period-10 motion ($z=7/10$) for $\eta=0.716$ ($\lambda_1=-0.015$, $\lambda_2=-0.091$); (b) period-16 motion ($z=14/16$) for $\eta=0.735$ ($\lambda_1=-0.003$, $\lambda_2=-0.108$); (c) period-8 motion ($z=7/8$) for $\eta=0.736$ ($\lambda_1=-0.007$, $\lambda_2=-0.105$).

$[0.650 \div 0.695]$ when there is no collision in the system, and thus the Lyapunov exponents $\lambda_1 = \lambda_2 = -0.05$ (their absolute total value is equal to the damping coefficient). For the range $\eta \in [0.696 \div 0.712]$, the hysteresis phenomenon is observed. The increase in the parameter η leads to an impactless motion (Fig. 4a), while the decrease in η results in a chaotic motion first ($\eta \in [0.698 \div 0.712]$, see Fig. 5b) and a period-2 motion afterwards ($\eta \in [0.696 \div 0.697]$, $z = 1/2$, see Fig. 4b). Thus, we can conclude that the following solutions coexist in the identified hysteresis region: an impactless motion with an impact period-2 motion (Fig. 4) as well as an impactless motion with a chaotic motion (Fig. 5). In the range $\eta \in [0.713 \div 0.950]$, regardless of the direction of change of the control parameter, the system exhibits the same dynamic behavior. We can observe a period-10 window ($z = 7/10$, Fig. 6a) within the range of chaotic behavior $\eta \in [0.713 \div 0.734]$ first and then a reverse period doubling cascade with period-16 motion for $\eta = 0.735$ ($z = 14/16$, Fig. 6b), period-8 motion for $\eta \in [0.736 \div 0.737]$ ($z = 7/8$, Fig. 6c), period-4 motion for $\eta \in [0.738 \div 0.743]$ ($z = 4/4$, see [30]), period-2 motion for $\eta \in [0.744 \div 0.919]$ ($z = 2/2$ and $z = 1/2$, see [30]) and period-1 motion for $\eta \in [0.920 \div 0.950]$ ($z = 1/1$, see [30]). Decreasing the frequency η from 0.925 (Fig. 7a, $z = 1/1$) until the value 0.919656 we can see that both eigenvalues of the Jacobi matrix ($0.609338 \pm 0.365643i$) are located inside the unit circle in the complex plane, while for $\eta = 0.919655$ a single real eigenvalue passes through the point (-1.0) of the unit circle. As a result of this bifurcation, a periodic solution of period $2T$ ($z = 2/2$) appears. Its phase plane is shown in Fig. 7b.

When analyzing the presented diagrams of spectra of Lyapunov exponents, it was noticed that not only do they confirm the results of earlier work by Pust and Peterka [30], but also allow for a more detailed analysis of the system dynamics and identification of attractors which were not detected by other methods in the above-cited work. For example, the period-10 window as well as the period-16 and period-8 solutions, expanding the period-doubling cascade range, were treated in [30] as irregular behaviors.

Now we compare the dynamical behavior of two systems with impacts which are equivalent in the sense of the same rate of impact energy dissipation: a system with Hertz's impacts described by Eqs. (7a) (or (7b) with $b_H = 0$) and a system with hard impacts described by the same equations but supplemented with impact condition (28) with $k_r = 1$. Fig. 8 presents the bifurcation diagrams of displacements (a) and Lyapunov exponents (b) for the system with Hertz contact model (Eqs. (6a) and (6b)) and parameters $b = 0.05$, $\rho = 2$, $k_H = 100$, $b_H = 0$ and $\xi = 1$. Their analysis reveals the following behaviors of the system: an impactless motion for $[0.65 \div 0.705]$, a hysteresis in the narrow region $[0.706 \div 0711]$, a chaotic motion for $[0.712 \div 0.737]$, and then a reverse period-doubling cascade with impact period-16 oscillations for $\eta = 0.738$ ($z = 14/16$), period-8 oscillations for $\eta = 0.739$ ($z = 7/8$), period-4 oscillations for $\eta \in [0.740 \div 0.745]$ ($z = 4/4$), period-2 oscillations for $\eta \in [0.746 \div 0.929]$ ($z = 2/2$ first and then $z = 1/2$) and period-1 oscillations for $\eta \in [0.930 \div 0.950]$ ($z = 1/1$). The mentioned hysteresis phenomenon evidences the smooth transition from the regular regime to the chaotic regime since an

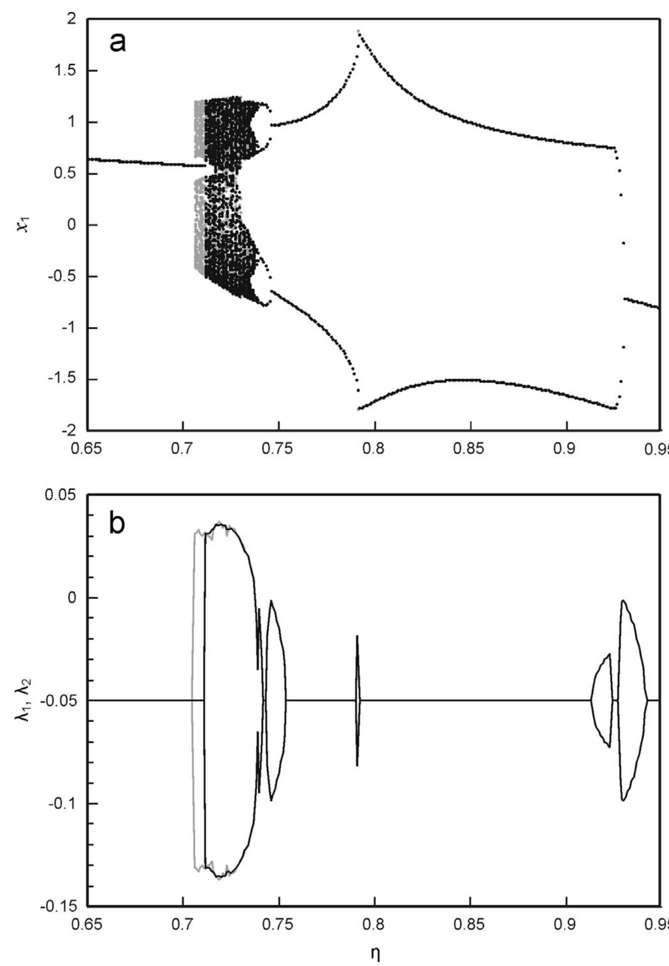

Fig. 8. Bifurcation diagrams of displacements x_1 (a) and corresponding spectra of Lyapunov exponents λ_1, λ_2 (b) for Hertz's impact model: $b = 0.05$, $\rho = 2$, $k_H = 100$, $b_H = 0$ and $\xi = 1$; $\Delta\eta = 0.001$.

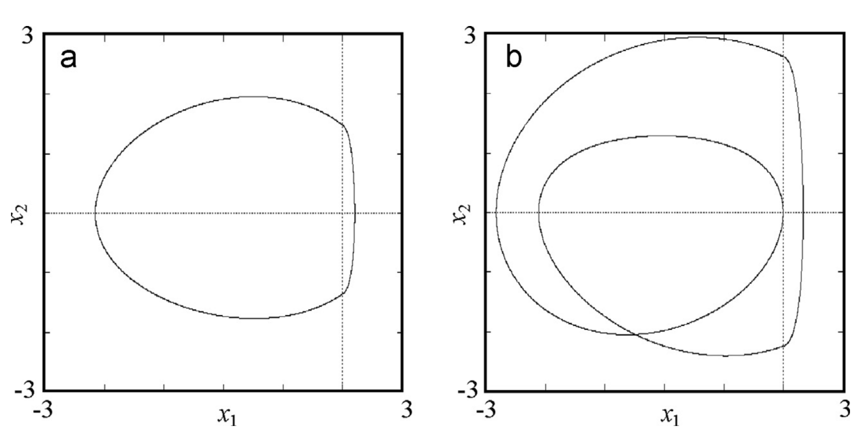

Fig. 7. Phase trajectories of periodic solutions for $b = 0.05$, $\rho = 2$, $k_H = 100$, $b_H = 0.1$ and $\xi = 1$: (a) period-1 motion ($z = 1/1$) for $\eta = 0.925$ ($\lambda_1 = -0.009$, $\lambda_2 = -0.125$); (b) period-2 motion ($z = 1/2$) for $\eta = 0.91$ ($\lambda_1 = -0.066$, $\lambda_2 = -0.066$).

impactless motion is recorded for $\eta \in [0.706 \div 0.710]$, a period-1 motion with impacts is detected for $\eta = 0.711$, while a chaotic motion is identified starting from $\eta = 0.712$. Fig. 9 depicts the displacement (a) and Lyapunov exponents (b) as functions of η for the same system as in Fig. 8 but for the range of η equal to $[0.7051 \div 0.7121]$ and the step $\Delta\eta = 0.0001$. For increasing values of η we observe an impactless motion until $\eta = 0.7109$ ($\lambda_1 = \lambda_2 = -0.05$), a period-1 motion with impacts for $\eta \in [0.7110 \div 0.7112]$ (for $\eta = 0.711$: $\lambda_1 = -0.04995$, $\lambda_2 = -0.05005$; for $\eta = 0.7111$: $\lambda_1 = -0.02479$, $\lambda_2 = -0.07521$; for $\eta = 0.7112$: $\lambda_1 = -0.00838$, $\lambda_2 = -0.09162$), a period-2 motion with impacts for $\eta = 0.7113$ ($\lambda_1 = -0.00549$, $\lambda_2 = -0.09451$) and a chaotic motion region for $\eta \geq 0.7114$ (for $\eta = 0.7114$: $\lambda_1 = 0.02813$, $\lambda_2 = -0.12813$), in which a period-24 window ($\eta = 0.7116$, $\lambda_1 = -0.00525$, $\lambda_2 = -0.09475$) is identified. For decreasing values of the control parameter, we detect chaotic behaviors first and then starting from $\eta = 0.7057$ we observe impactless oscillations.

It is worth to point out that in the case when there is no loss of energy during the collision in the system (Fig. 8, $b_H = 0$), the general structure of bifurcation diagrams (the sequence of bifurcations) is identical as in the case when there is such a loss of energy (Fig. 3, $b_H = 0.1$). Fig. 10 presents the displacement (a) and the Lyapunov exponents (b) as the functions of the excitation frequency for the system (Eqs. (6a) and (6b)) with hard impact model and the following parameters $b = 0.05$, $\rho = 2$, $k_r = 1$ and $\xi = 1$. In this system, there is clearly no loss of energy during the impacts. Comparing the graphs of Fig. 10 with the corresponding graphs of Figs. 8 and 9, we observe not only their qualitative but also quantitative agreement. This agreement manifests itself in the appearance, for almost the same values of the excitation force, of the chaotic and periodic solutions with almost identical values of both the corresponding Lyapunov exponents. Fig. 11a shows such a chaotic solution of the system with Hertz type collisions for $b_H = 0$ and $\eta = 0.7114$ ($\lambda_1 = 0.02813$, $\lambda_2 = -0.12813$), while Fig. 11b depicts a corresponding chaotic solution of the system with Newton type collisions for $k_r = 1$ and $\eta = 0.711$ ($\lambda_1 = 0.030$, $\lambda_2 = -0.130$). It can be concluded that when the two systems begin to come into collisions within the chaotic zones, then the corresponding rates of divergence of adjacent trajectories are almost identical, irrespective of the model of collision chosen. This is evidenced by very close values of Lyapunov exponents. In the case of the system with Hertz's impacts and $b_H = 0$, the chaotic motion disappears through reverse period doubling cascade, in which for $\eta = 0.738$ we record a periodic motion with period 16 (Fig. 12a, $\lambda_1 = -0.010$, $\lambda_2 = -0.090$). In the case of the system with Newton's impacts and $k_r = 1$, the chaotic behavior disappears for similar value of the frequency $\eta = 0.733$, but bifurcating to a period-3 motion (Fig. 12b, $\lambda_1 = -0.013$, $\lambda_2 = -0.087$). In addition, in this case a period-16 motion was observed for $\eta = 0.740$ (Fig. 12c, $\lambda_1 = -0.003$, $\lambda_2 = -0.097$). Other significant similarities between these systems' behavior include: a periodic motion with period 4 ($z = 4/4$) of the system with Hertz model of contact ($b_H = 0$) for $\eta \in [0.740 \div 0.745]$ and the system with Newton's contact model ($k_r = 1$) for $\eta \in [0.741 \div 0.745]$, as well as a periodic motion with period 2 ($z = 2/2$ first and then $z = 1/2$) of both the systems for a wide range of the control parameter

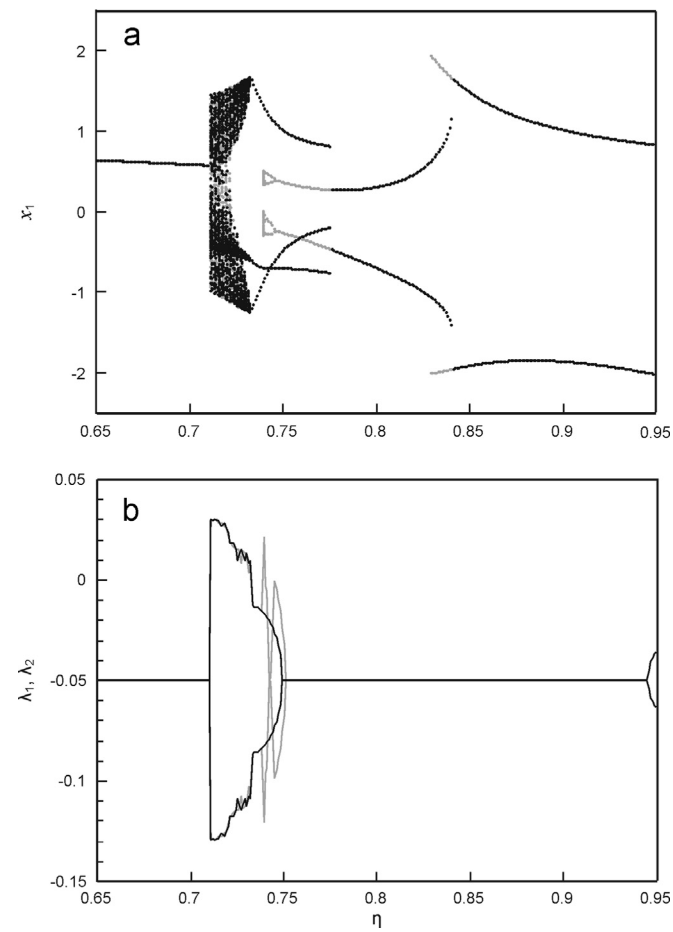

Fig. 10. Bifurcation diagrams of displacements x_1 (a) and corresponding spectra of Lyapunov exponents λ_1, λ_2 (b) for hard impact model: $b = 0.05$, $k_r = 1$ and $\xi = 1$; $\Delta\eta = 0.001$.

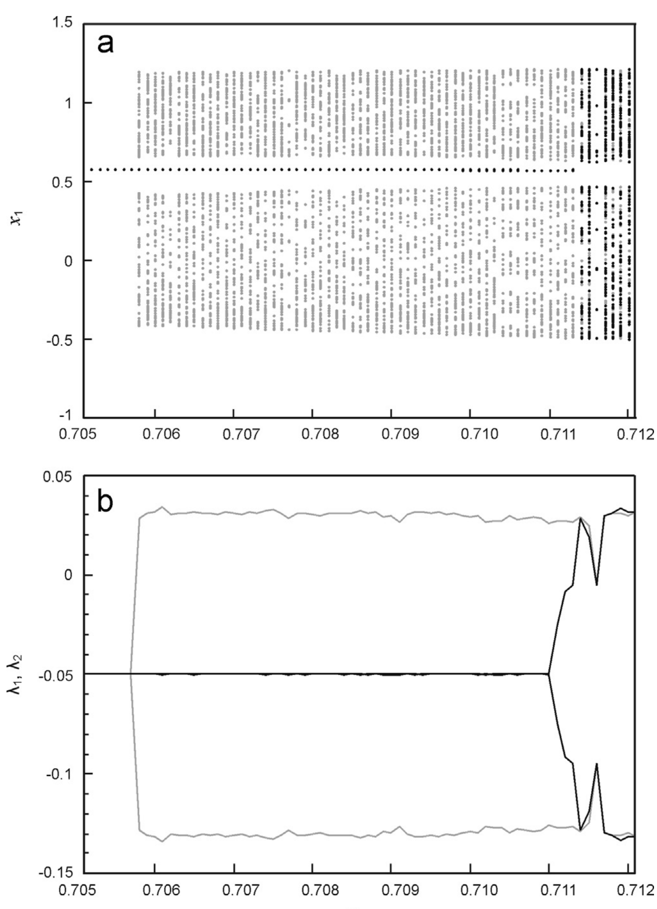

Fig. 9. Bifurcation diagrams of displacements x_1 (a) and corresponding spectra of Lyapunov exponents λ_1, λ_2 (b) for Hertz's impact model: $b = 0.05$, $\rho = 2$, $k_H = 100$, $b_H = 0$ and $\xi = 1$; $\Delta\eta = 0.0001$.

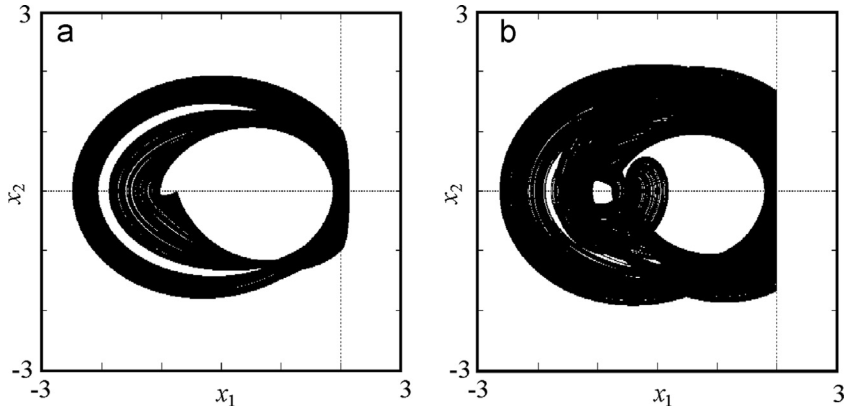

Fig. 11. Chaotic solutions of the system with parameters $b=0.05$, $\rho=2$, $\xi=1$: (a) Hertz's type contact model, $\eta=0.7114$, $k_H=100$, $b_H=0$ ($\lambda_1=0.02813$, $\lambda_2=-0.12813$); (b) Newton's contact model, $\eta=0.711$, $k_r=1$ ($\lambda_1=0.030$, $\lambda_2=-0.130$).

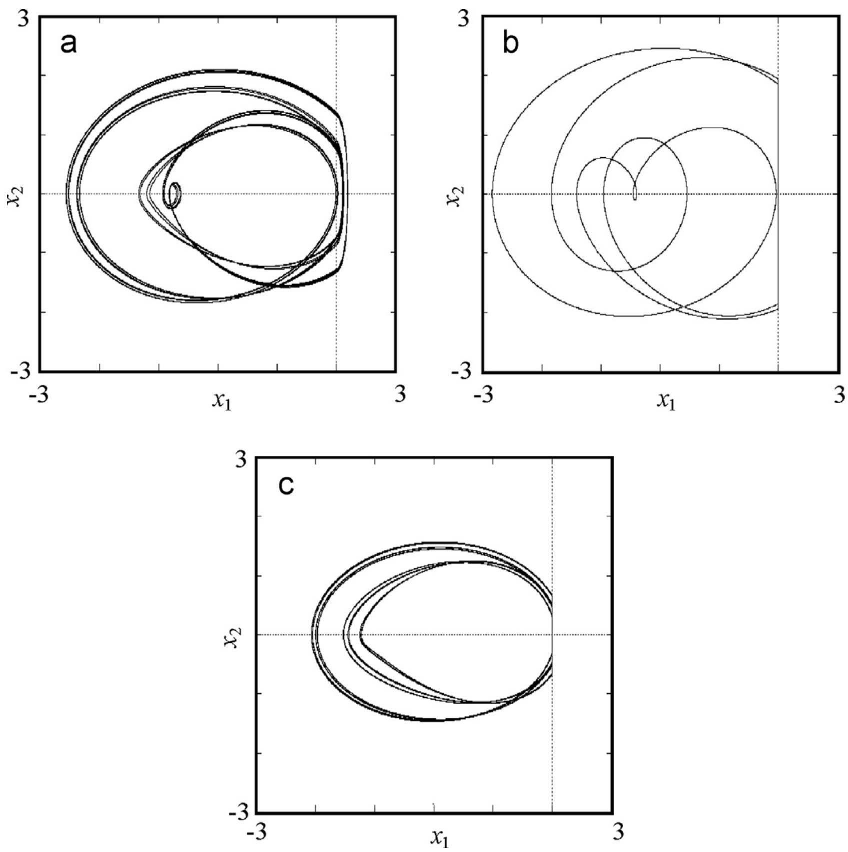

Fig. 12. Periodic solutions of the system with parameters $b=0.05$, $\rho=2$, $\xi=1$: (a) Hertz's type contact model, period-16 motion ($z=14/16$) for $\eta=0.738$, $k_H=100$, $b_H=0$ ($\lambda_1=0.010$, $\lambda_2=-0.090$); (b) Newton's contact model, period-3 motion ($z=2/3$) for $\eta=0.733$, $k_r=1$ ($\lambda_1=0.013$, $\lambda_2=-0.087$); (c) Newton's contact model, period-16 motion ($z=16/16$) for $\eta=0.740$, $k_r=1$ (e.g. for the initial conditions $x_1=-0.042$, $x_2=-1.081$; $\lambda_1=0.003$, $\lambda_2=-0.097$).

η. Some examples of such similarities are illustrated in Fig. 13 (in the case of hard impacts the period-4 solution co-exists with a period-3 solution), Fig. 14 (in the case of hard impacts the period-2 solution co-exists with a period-3 solution) and Fig. 15 (in the case of hard impacts the period-2x; solution co-exists with a period-3 solution). A period-1 solution of the system with Newton's model of contact with $k_r=1$ can be observed for $\eta>0.95$. Finally, it is worth noting that in the case of the considered system with perfectly elastic hard impacts the absolute value of the aggregate sum of the Lyapunov exponents is equal to the value of damping coefficient, just as it is in the case of the system with undamped Hertz type impacts.

6. A mechanical engineering application: beam system with impacts

Structural elements such as beams are perhaps the most commonly used elements of engineering design (buildings, bridges, aircraft, wind turbines). The dynamics of beams involving amplitude constraint barriers was extensively studied in the literature (see, for example, [23,31,38,39]). The results of Section 5 enrich these results in the case of linear beam model. In particular, the revealed qualitative and quantitative agreement (in the sense of almost identical values of the Lyapunov exponents) of dynamical

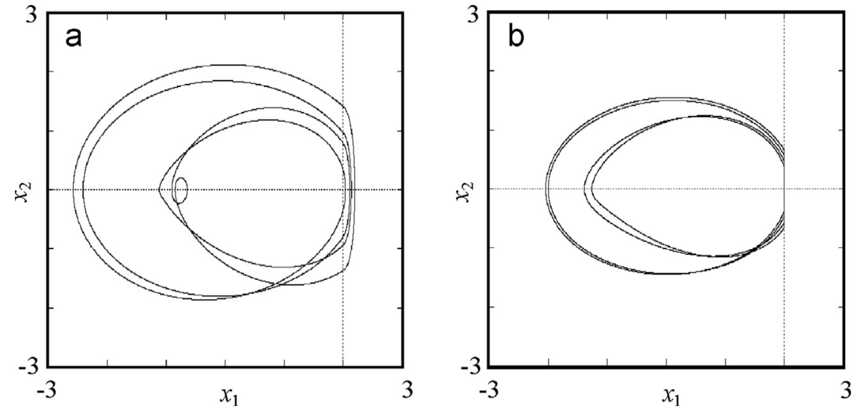

Fig. 13. Periodic solutions with period 4 ($z=4/4$) of the system with parameters $\eta=0.744$, $b=0.05$, i$=2$, $\xi=1$: (a) Hertz's type contact model with $k_H=100$, $b_H=0$ ($\lambda_1=-0.019$, $\lambda_2=-0.081$); (b) Newton's contact model with $k_r=1$ (e.g. for the initial conditions $x_1=-0.169$, $x_2=-0.962$; $\lambda_1=-0.017$, $\lambda_2=-0.083$).

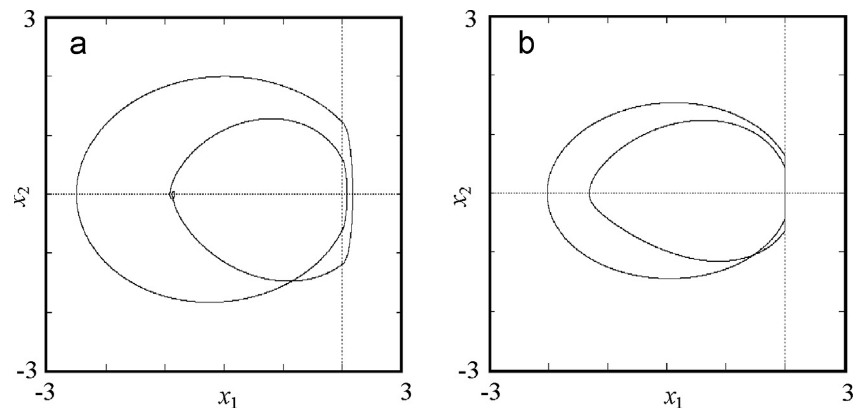

Fig. 14. Periodic solutions with period 2 ($z=2/2$) of the system with parameters $\eta=0.746$, $b=0.05$, $\rho=2$, $\xi=1$: (a) Hertz's type contact model with $k_H=100$, $b_H=0$ ($\lambda_1=-0.001$, $\lambda_2=-0.099$); (b) Newton's contact model with $k_r=1$ (e.g. for the initial conditions $x_1=-0.237$, $x_2=-0.887$; $\lambda_1=-0.005$, $\lambda_2=-0.095$).

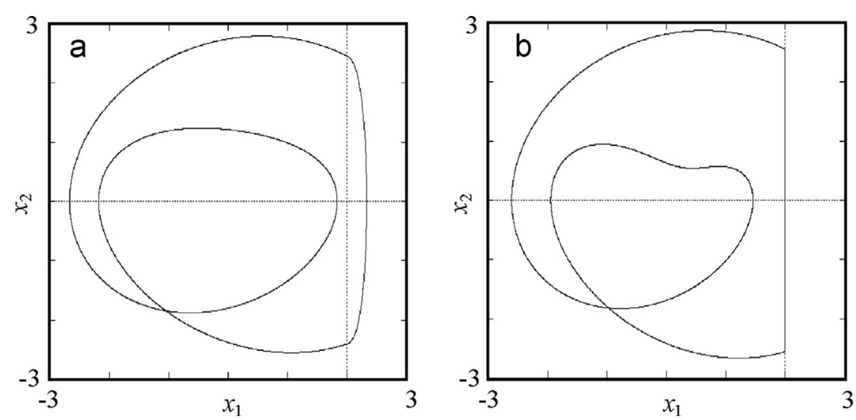

Fig. 15. Periodic solutions with period 2 ($z=1/2$) of the system with parameters $\eta=0.9$, $b=0.05$, $\rho=2$, $\xi=1$: (a) Hertz's type contact model with $k_H=100$, $b_H=0$ ($\lambda_1=-0.050$, $\lambda_2=-0.050$); (b) Newton's contact model with $k_r=1$ ($\lambda_1=-0.050$, $\lambda_2=-0.050$).

behaviors of a system with Hertz type undamped collisions of relatively small values of stiffness and a system with perfectly elastic hard collisions, holds true in the important case when the two systems begin to come into collisions with low velocity, which causes instabilities of grazing-type. However, as it was established by Emans et al. [38], if the beams are parts of larger system, then for physically realistic parameters, significant errors in the dynamic responses can result from neglecting even small nonlinearities. In this section we extend the studies of Emans et al. [38] and Lin et al. [39] on the compound effect of the nonlinearities due to beam deflection and linear barrier to the case of other barrier models.

Consider a simple cantilever beam system shown in Fig. 16, consisting of a mass M and two leaf springs of length L and bending stiffness EI. The mass is excited by a force F_0 and the boundary conditions prevent its rotation. This beam arrangement is commonly used as a typical structural element in buildings, with the mass representing a floor.

According to the precise nonlinear approximation for beam reaction established in [38], the equation of motion for the beam system from Fig. 16 accompanied with the linear barrier is as follows:

$$M\frac{d^2x}{dt^2}+c\frac{dx}{dt}+\frac{12EI}{L^3}x+\frac{432EI}{35L^5}x^3+F_\rho=F_0\cos\omega t, \tag{27}$$

where the collision force F_ρ is of the form:

$$F_\rho = 0 \quad x < \rho$$
$$F_\rho = k_s(x-\rho) \quad x \ge \rho, \tag{28}$$

in which k_s denotes the stiffness of the spring. The corresponding first order nondimensional equations can be written as

$$\dot{x}_1 = x_2$$
$$\dot{x}_2 = \xi \cos \eta\tau - 2bx_2 - x_1 - \beta x_1{}^3 - F_r, \tag{29}$$

where

$$F_r = 0 \quad x_1 < r$$
$$F_r = k_S(x_1 - r) \quad x_1 \ge r, \tag{30}$$

and $x_1 = x/L$, $\tau = \alpha t$, $\alpha = \sqrt{k_l/M}$, $k_l = 12EI/L^3$, $b = c/(2\sqrt{k_l m})$, $\xi = F_0/(\alpha^2 ML)$, $\eta = \omega/\alpha$, $\beta = 36/35$, $r = \rho/L$, $k_S = k_s/k_l$.

Detailed analysis of physically realistic responses provided in [38] revealed qualitative differences in behavior between the linear ($\beta = 0$) and the nonlinear ($\beta = 36/35$) beam systems with

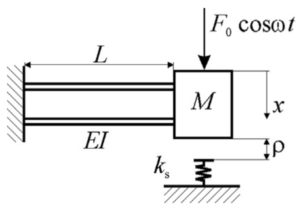

Fig. 16. Beam system with impacts.

linear elastic impacts. We show that this is also the case for beam systems with Hertz's and Newton's impacts, i.e. the system described by (29) with the collision force

$$F_r = 0 \quad x_1 < r$$
$$F_r = k_H(x_1 - r)^{3/2} \quad x_1 \ge r, \tag{31}$$

in which $k_H = (k_h\sqrt{L})/k_l$, and the system described by (29) with $F_r = 0$ supplemented with impact condition (26), respectively.

We compare the dynamical behavior of three systems with impacts which are equivalent in the sense of the same rate of impact energy dissipation. Let us choose the following realistic values of the parameters $b = 0.026$, $\xi = 0.08$, $\eta = 0.554$ and $\rho = 0.079$, which lead to low amplitude oscillations (cf. [38]). Consider first the nonlinear case $\beta = 36/35$ and the linear case $\beta = 0$ of the beam system (29) with soft impacts of Hertz's type (31) with $k_H = 100$. Fig. 17a shows the Poincare map of a chaotic orbit (the Lyapunov exponents: $\lambda_1 = 0.01455$, $\lambda_2 = -0.06650$) for $\beta = 36/35$, while Fig. 17b depicts a period-6 solution ($\lambda_1 = -0.02546$, $\lambda_2 = -0.02654$) for $\beta = 0$. For the same values of the parameters, similar results are obtained in the case when the impacts are modeled by Newton's law with the restitution coefficient $k_r = 1$. Chaotic motion shown in Fig. 18a ($\lambda_1 = 0.02364$, $\lambda_2 = -0.07564$) corresponds to $\beta = 36/35$ while period-4 motion depicted in Fig. 18b ($\lambda_1 = -0.02588$, $\lambda_2 = -0.02612$) corresponds to $\beta = 0$. In the case of the collision model (30) (see, e.g., [13], [23]) the functions $\mathbf{f}_{2i-1}$ and $\mathbf{f}_{2i}$ in (13) and (16) are equal to $\mathbf{f}(x_1, x_2) = (x_2, \xi \cos \eta\tau - 2bx_2 - x_1 - \beta x_1{}^3 - F_r)$ with $F_r = 0$ and $F_r = k_S(x_1 - r)$, respectively. Then the Jacobi matrices of the transition functions $\mathbf{h}(\mathbf{x}) = x_1 - r$ and $\mathbf{g}(\mathbf{x}) = [x_1, x_2]$ are also

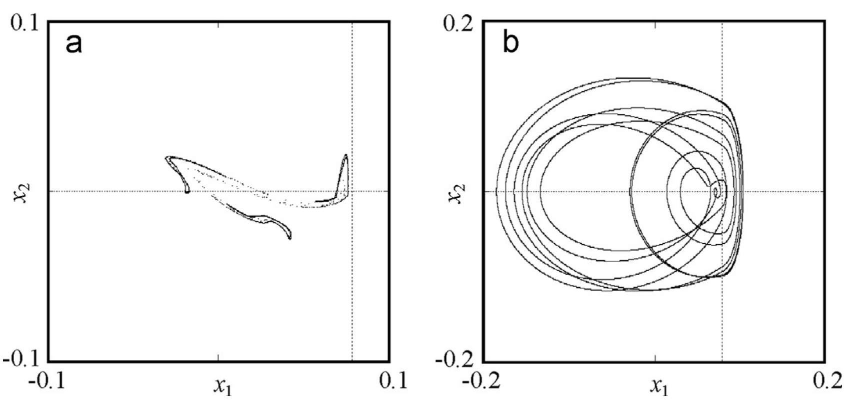

Fig. 17. A comparison between (a) piecewise nonlinear and (b) piecewise linear beam system responses calculated for $b = 0.026$, $\xi = 0.08$, $\eta = 0.554$, $\rho = 0.079$ and $k_H = 100$; (a) shows a Poincare map forming a strange attractor ($\lambda_1 = 0.01455$, $\lambda_2 = -0.06650$), while (b) depicts a period-6 response with 8 impacts per period in the form of a phase plane ($\lambda_1 = -0.02546$, $\lambda_2 = -0.02654$).

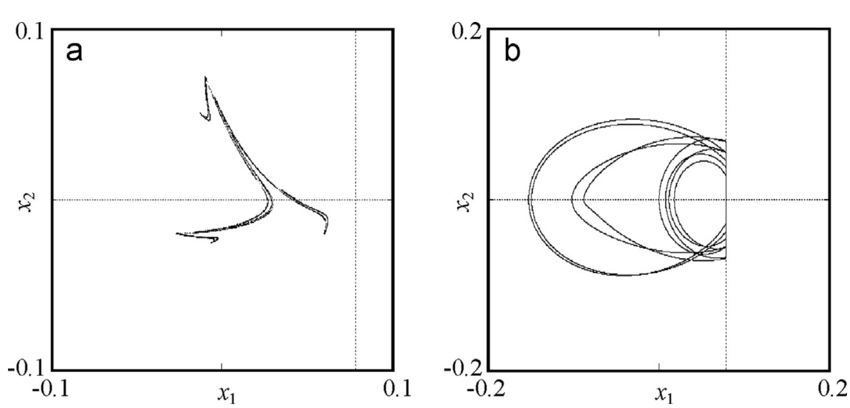

Fig. 18. A comparison between (a) piecewise nonlinear and (b) piecewise linear beam system responses calculated for $b = 0.026$, $\xi = 0.08$, $\eta = 0.554$, $\rho = 0.079$ and $k_r = 1$; (a) shows a Poincare map forming a strange attractor ($\lambda_1 = 0.02364$, $\lambda_2 = -0.07564$), while (b) depicts a period-4 with 8 impacts per period in the form of a phase plane ($\lambda_1 = -0.02588$, $\lambda_2 = -0.02612$).

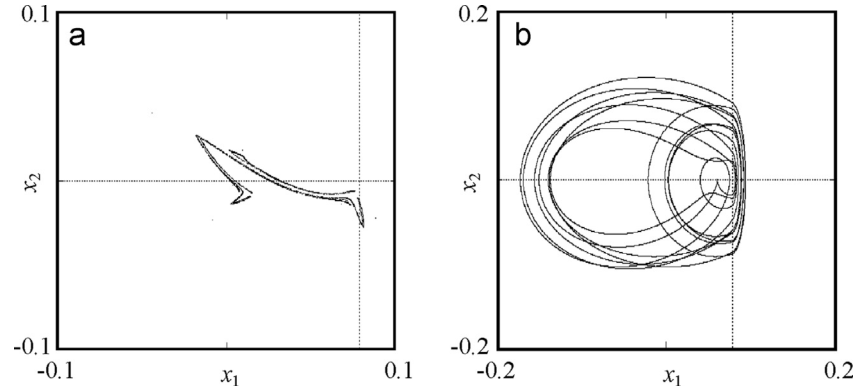

Fig. 19. A comparison between (a) piecewise nonlinear and (b) piecewise linear beam system responses calculated for $b=0.026$, $\xi=0.08$, $\eta=0.554$, $\rho=0.079$ and $k_S=25$; (a) shows a Poincare map forming a strange attractor ($\lambda_1=0.00293$, $\lambda_2=-0.05493$), while (b) depicts a period-7 with 11 impacts per period in the form of a phase plane ($\lambda_1=-0.02600$, $\lambda_2=-0.02600$).

given by (24) and (25), and the values of the perturbations immediately after and immediately before the instant of singularity are related as in (23). Fig. 19a presents the Poincare map of a chaotic solution (the Lyapunov exponents take the values $\lambda_1=0.00293$, $\lambda_2=-0.05493$) for the nonlinear beam model with $\beta=36/35$ and $k_S=25$, while Fig. 19b shows a period-7 solution ($\lambda_1=-0.02600$, $\lambda_2=-0.02600$) for the linear beam model ($\beta=0$) with the same value of k_S. Similar effects have also been observed for other values of the clearance ρ as well as for other values of impact parameters (cf. de Souza et al. [25], Emans et al. [38] and Lin et al. [39]).

7. Conclusions

In this paper, investigations of a one degree of freedom impact oscillator with a Hertz type and Newton type one-sided amplitude constraint have been presented. This model is commonly used to describe the behavior of beams, which constitute basic elements of engineering design. The obtained results allow the following conclusions.

The occurrence of a barrier with a certain vulnerability (elastic-damping Hertz's type stop) in a relatively simple mechanical system causes the appearance of complex nonlinear behaviors like bifurcations and chaos. The greatest range of chaotic behavior takes place for the dimensionless clearance equal to 2. A significant impact on the nature of system's behavior has the frequency of the exciting force.

Müller's procedure and the classical algorithm of Benettin et al. enable determining the spectrum of Lyapunov exponents for systems with a barrier of Hertz's, Newton's as well as linear elastic type. The knowledge of bifurcation diagrams of the spectra of Lyapunov exponents allows a thorough analysis of the qualitative changes of motion of the system which results in identification of attractors which have not been reported on the basis of bifurcation diagrams of displacements in [30].

The Hertz damp system manifests hysteretic features in its transition from impactless motion to impact motion, namely an impactless motion coexists with a period-2 impact motion. Other characteristic features of systems' behavior include a period-16 window within a chaotic region as well as the classical period-doubling cascade firstly bifurcating to a period-2, secondly to a period-4, then to a period-8 and eventually settling to a period-16 motion.

The dynamics of a system with Hertz type undamped collisions, even at relatively small values of stiffness, shows a good qualitative and quantitative agreement with the dynamics of an equivalent system with perfectly elastic hard collisions. This agreement manifests itself in the appearance, for almost the same values of the excitation force, of the chaotic motions with identical values of both the corresponding Lyapunov exponents as well as in the existence, in a wide range of the control parameter, of periodic motions with impacts for which the corresponding Lyapunov exponents are very close to each other. In particular, this is the case when the two systems begin to come into collisions with low velocity impacts, resulting in instabilities of grazing-type.

The comparison of dynamic responses of simple linear and nonlinear cantilever beam systems with impacts of Hertz's and Newton's type revealed their qualitative differences for physically realistic parameters. In the case of the linear elastic impact model this effect was established in [38].

Acknowledgment

This study has been supported by the Polish National Science Center (NCN) under Project no DEC-2012/05/B/ST8/00057. Authors kindly acknowledge this support.

References

[1] Oseledec VI. A multiplicative ergodic theorem: lyapunov characteristic numbers for dynamical systems. Trans Moscow Math Soc 1968;19:197–231.
[2] Benettin G, Galgani L, Giorgilli A, Strelcyn JM. Lyapunov exponents for smooth dynamical systems and hamiltonian systems; a method for computing all of them, part I: theory, part II: numerical application. Meccanica 1980;15:9–30.
[3] Shimada I, Nagashima T. A numerical approach to ergodic problem of dissipative dynamical systems. Prog Theor Phys 1979;61(6):1605–16.
[4] Parker TS, Chua LO. Practical numerical algorithms for chaotic systems. New York: Springer-Verlag; 1989.
[5] Oestreich M, Hinrichs N, Popp K. Bifurcation and stability analysis for a non-smooth friction oscillator. Arch Appl Mech 1996;66:301–14.
[6] Stefanski A. Estimation of the largest Lyapunov exponent in systems with impacts. Chaos Solitons Fractals 2000;11(15):2443–51.
[7] Dabrowski A. Estimation of the largest Lyapunov exponent from the perturbation vector and its derivative dot product. Nonlinear Dyn 2012;67:283–91.
[8] Takens F. Detecting strange attractors in turbulence. Lect Notes Math 1981;898:366.
[9] Wolf A, Swift JB, Swinney HL, Vastano JA. Determining Lyapunov exponents from a time series. Physica D 1985;16:285–317.
[10] Parlitz U. Identification of true and spurious Lyapunov exponents from time series. Int J Bifurc Chaos 1992;2:155–65.
[11] Sano M, Sawada Y. Measurement of the Lyapunov spectrum from a chaotic time series. Phys Rev Lett 1985;55(10):1082–5.
[12] Yang C, Wu CQ. A robust method on estimation of Lyapunov exponents from a noisy time series. Nonlinear Dyn 2011;64:279–92.
[13] Müller PC. Calculation of Lyapunov exponents for dynamical systems with discontinuities. Chaos Solitons Fractals 1995;5(9):1671–81.
[14] Aizerman MA, Gantmakher FR. On the stability of periodic motions. J Appl Math Mech 1958;22:1065–78.
[15] Nordmark AB. Non-periodic motion caused grazing incidence in an impact oscillator. J Sound Vib 1991;145:279–97.

[16] Jin L, Lu QS, Twizell EH. A method for calculating a spectrum of Lyapunov exponents by local maps in non-smooth impact-vibrating systems. J Sound Vib 2006;298(4–5):1019–33.

[17] De Souza SLT, Caldas IL. Calculation of Lyapunov exponents in systems with impacts. Chaos Solitons Fractals 2004;19:569–79.

[18] Galvanetto U. Numerical computation of Lyapunov exponents in discontinuous maps implicitly defined. Comput Phys Commun 2000;131:1–9.

[19] Brogliotо B. Nonsmooth mechanics. London: Springer; 1999.

[20] Shaw SW, Holmes PJ. A periodically forced piecewise linear oscillator. J Sound Vib 1982;90(1):129–55.

[21] Goldsmith W. Impact: theory and physical behavior of colliding solids. London: Edward Arnold; 1960.

[22] Blazejczyk-Okolewska B, Czolczynski K, Kapitaniak T. Hard versus soft impacts in oscillatory systems moddeling. Commun Nonlinear Sci Numer Simul 2010;15(5):1358–67.

[23] Blazejczyk-Okolewska B, Czolczynski K, Kapitaniak T. Dynamics of a Two-degree-of-freedom cantilever beam with impacts. Chaos Solitons Fractals 2009;40(4):1991–2006.

[24] Blazejczyk-Okolewska B, Czolczynski K, Kapitaniak T. The effect of discretization on the numerical simulation of the vibrations of the impacting cantilever beam. Commun Nonlinear Sci Numer Simul 2010;15(10):3073–90.

[25] De Souza SLT, Wiercigroch M, Caldas IL, Balthazar JM. Suppressing grazing chaos in impacting system by structural nonlinearity. Chaos Solitons Fractals 2008;38:864–9.

[26] Ing J, Pavlovskaia E, Wiercigroch M, Banerjee S. Experimental study of impact oscillator with one-sided elastic constraint. Philos Trans R Soc A 2008;366:679–704.

[27] Ing J, Pavlovskaia E, Wiercigroch M, Banerjee S. Bifurcation analysis of an impact oscillator with a one-sided elastic constraint near grazing. Physica D 2010;239:312–21.

[28] Wiercigroch M, Sin VWT. Experimental Study of a Symmetrical Piecewise Base-Excited Oscillator. J Appl Mech 1998;65:657–63.

[29] Foale S, Bishop SR. Bifurcations in impact oscillators. Nonlinear Dyn 1994;6:285–99.

[30] Pust L, Peterka F. Impact oscillator with Hertz's model of contact. Meccanica 2003;38(1):99–114.

[31] Ibrahim RA. Vibro-impact dynamics, modeling, mapping and applications. Berlin Heidelberg: Springer-Verlag; 2009.

[32] Li Q, Chen Y, Wei Y, Lu Q. The analysis of the spectrum of Lyapunov exponents in a two-degree-of-freedom vibro-impact system. Int J Non-Linear Mech 2011;40:197–203.

[33] Li QH, Tan JY. Lyapunov exponent calculation of a two-degree-offreedom vibro-impact system with symmetrical rigid stops. Chin Phys B 2011;20(4):1–9.

[34] Luo G, Ma L, Lv X. Dynamic analysis and suppressing chaotic impacts of a two-degree-of-freedom oscillator with a clearance. Nonlinear Anal: Real World Appl 2009;10:756–78.

[35] Yue Y. The dynamics of a symmetric impact oscillator between two rigid stops. Nonlinear Anal: Real World Appl 2011;12:741–50.

[36] Yue Y, Xie J. Lyapunov exponents and coexistence of attractors in vibro-impact systems with symmetric two-sided rigid constraints. Phys Lett A 2009;373:2041–6.

[37] Andreaus U, Placidi L, Rega G. Numerical simulation of the soft contact dynamics of an impacting bilinear oscillator. Commun Nonlinear Sci Numer Simul 2010;15:2603–16.

[38] Emans J, Wiercigroch M, Krivtsov AM. Cumulative effect of structural nonlinearities: chaotic dynamics of cantilever beam system with impacts. Chaos Solitons Fractals 2005;23:1661–70.

[39] Lin W, Qiao N, Yuying H. Bifurcations and chaos in a forced cantilever system with impacts. J Sound Vib 2006;296:1068–78.

[40] Bazhenov VA, Pogorelova OS, Postnikova TG, Lukyanchenko OA. Numerical investigations of the dynamic processes in vibroimpact systems in modeling impact by a force of contact interaction. Strength Mater 2008;40:656–62.

[41] Bichri A, Belhag M, Perret-Liaudet J. Control of vibroimpact dynamics of a single-sided Hertzian contact forced oscillator. Nonlinear Dyn 2011;63:51–60.